

Published in:

èScripta Materialia, vol. 69 issue 6, September 2013, Pages 469–472

<http://dx.doi.org/10.1016/j.scriptamat.2013.05.044>

## The Plasticity Size Effect in Replicated Microcellular Aluminium

R Goodall<sup>1\*</sup>, J-F Despois<sup>2</sup> and A Mortensen

Ecole Polytechnique Fédérale de Lausanne (EPFL), Laboratory for Mechanical Metallurgy, MX-D Ecublens 141, Station 12, CH-1015 Lausanne, Switzerland

1 Present address: Dept. Materials Science and Engineering, University of Sheffield, Mappin St, Sheffield, S1 3JD UK, r.goodall@sheffield.ac.uk

2 Present address: Novelis Switzerland SA, Rte des Laminoirs 15, CH - 3960 Sierre, Switzerland

\*: Corresponding author

### Abstract

Microcellular aluminium can be produced by replication with pores across a wide range of sizes but otherwise identical structures. Compressive tests reveal a plasticity size effect, with samples showing higher strengths and higher rates of work hardening for smaller pore diameters. This size effect is shown to be dislocational, its main origin being dislocation emission during the composite stage of foam processing.

**Keywords:** Foams; Compression Test; Dislocation Theory; Size Effect

The plastic flow stress of metals often becomes size-dependant when this falls below roughly 10  $\mu\text{m}$ : beyond this point, the finer the microstructure or size of a deforming metal, the higher its flow stress. The effect has been documented in many configurations, ranging from wire torsion [1], FIB-milled micropillar compression [2, 3], nanoindentation [4], dispersion and grain boundary hardening [5, 6], to the flow stress of metal matrix composites [7, 8], metal microparticles [9] or thin films [6, 10].

Plasticity size effects are also manifest in porous metals: when pores of a microcellular metal decrease below a certain size (all else constant) its flow stress starts increasing [11]. Microcellular aluminium is one of the most convenient materials for the study of this effect. The aluminium replication process, described in more detail in Ref. [12], consists of preparing a packed preform of NaCl particles, which is infiltrated with aluminium that is then solidified before leaching the salt. This leaves a network of interconnected aluminium struts, which delineate pores, of controlled size, shape and volume fraction. The flow stress of the resulting microcellular high-purity aluminium increases, all else constant, as the pore size falls below roughly 100  $\mu\text{m}$  [13-16]. The oxide layer covering the pores exerts a strong influence on its flow stress [17], and thermally activated slip in this material is altered by the free surfaces within it [16]. Here, we show that the plasticity size effect in these materials is dislocational in nature and that it has the same origin as in metal matrix composites.

Foams were made with 99.99% pure aluminium using NaCl particles crushed and sieved to produce size ranges with three different mean particle diameters, 400  $\mu\text{m}$ , 75  $\mu\text{m}$  or 26  $\mu\text{m}$ . The particles were packed and cold isostatically pressed to produce preforms. These were then infiltrated at 710°C under different argon gas pressures, chosen to drive uniform infiltration of the metal into the preform (0.4 MPa for 400  $\mu\text{m}$ , and 8 MPa for the other two sizes), and cooled slowly in the furnace before being machined. The salt was then removed by dissolution in ordinary tap water, significant corrosion being avoided by frequently changing the water and using the minimum amount of immersion time required. Note that, since a corrosion inhibitor was here not used during

NaCl dissolution, samples of this work are covered by a layer of oxide known to enhance the aluminium flow stress within the microcellular metal [17].

Resulting sample microstructures are shown in Fig. 1. Samples of foam of each pore size in the form of cylinders of 20 mm height and 20 mm diameter were produced, and tested in compression using a screw-driven testing machine with a constant cross head speed of  $0.005 \text{ mm s}^{-1}$ . Three LVDTs were positioned regularly around the specimen and used to measure the strain.

Replication typically produces microcellular metals that display the standard stress-strain curve for metal foams as described by Gibson and Ashby [18, 19], except that the plateau region is not of uniform stress. Rather, it displays a finite rate of work-hardening, which reflects dual influences of hardening in the metal making the foam, coupled with an absence of the collapse bands that are observed when most other metal foams are compressed [11, 16, 19-21]. Curves from samples of this work are shown in Fig. 2: the flow stress and rate of work hardening of the present microcellular metal are significantly raised as the pore size is reduced from 400 to 26  $\mu\text{m}$ . Similar trends for tension have been documented previously [13], showing that there is a clearly observable size effect in these foams. Note that samples in this investigation have all been treated in the same way for the dissolution step, and that even the one with the largest pore size (400 $\mu\text{m}$ ) contains in excess of 100,000 pores (with 50 of them expected along the shortest sample dimension, this being far in excess of the level usually required for data to be representative of the material free of sample edge effects [11, 19]). The plasticity size effect documented here is thus not due to variations in metal surface condition or to variations in the ratio of specimen size relative to pore size.

To identify the origin of this effect, additional cylinders of the same materials and same size were produced and taken through the treatments depicted schematically in Fig. 3. Treatment 1 involved the microcellular material being processed as before, and then annealed in flowing argon at  $500^\circ\text{C}$  for 2 hours. Treatment 2 was the conventional route used to make the first set of samples, outlined above, while Treatment 3 took the as-machined samples, with the NaCl still inside, and cooled them to liquid nitrogen temperatures ( $-196^\circ\text{C}$ ) before dissolving the salt at room temperature. All samples were then dried and tested in compression following the procedure previously described.

The first two treatments show the plasticity size effect is dislocational: it disappears in samples that have been annealed at high temperature after processing. This suggests that the size-effect is due to a high density of dislocations initially present in the metal when pores are small (if it were due to an oxide layer developed on the surface, for example, it would remain after annealing); transmission electron microscopy confirms this [16, 17]. This in turn raises the question of how a sufficient number of dislocations to cause hardening would be created in a sample that was processed through a solidification route. This is solved by analogy with metal matrix composites: before leaching, the metal is the matrix of a NaCl/Al composite. It is well known that when metal matrix composites are cooled from processing temperatures, differential thermal contraction between the metal and its reinforcing phase often causes significant dislocation emission within the metal [7, 8]. Here, NaCl particles indeed have a different thermal expansion coefficient than aluminium ( $\text{CTE}_{\text{NaCl}} = 4.05 \times 10^{-5} \text{ K}^{-1}$  [22] and  $\text{CTE}_{\text{Al}} = 2.36 \times 10^{-5} \text{ K}^{-1}$  [23]). Thermal phase strains therefore develop during cooling (note that here, unlike most ceramic reinforced metals, it is the metal that has the lower CTE: NaCl particles “pull” on the metal during cooldown, and emit vacancy loops). The purpose of the third treatment was to amplify this effect, by increasing the thermal excursion while the NaCl particles are still contained within aluminium.

To quantify the results, the foam stresses at 0.2%, 2% and 5% plastic deformation were measured for each sample, following the method used in Ref. [20]. This value is strongly affected by the foam relative density  $V_s$ , which in the present series of samples varied from 0.19 to 0.28. To remove this factor, we have simply scaled the microcellular metal yield or flow stress  $\sigma^*$  using a power-law relation deduced by a mean square regression of data for 400  $\mu\text{m}$  pore size replicated foams [24]:

$$\frac{\sigma^*}{\sigma_0} = 1.62V_s^{2.5} \quad (1)$$

where  $\sigma_0$  is the yield or flow stress of the dense metal (estimated for Al in 400  $\mu\text{m}$  Al foam by microindentation of larger foam struts in undeformed material). If the dislocations generated increase the metal strength according to the classical Taylor relationship, then the global density of dislocations in the (highly pure) aluminium,  $\rho_d$ , can be found through:

$$\rho_d = \left( \frac{\sigma_0}{\alpha_T G b} \right)^2 \quad (2)$$

where  $\alpha_T = 1.25$  for aluminium [25],  $b$  is the magnitude of the Burgers vector ( $2.86 \times 10^{-10}$  for Al) and  $G$  is the shear modulus (26 GPa for Al) [26].

The average surface-to-surface mean free path in the metal,  $\lambda$ , can also be calculated as a function of  $V_s$  and the pore diameter  $D$ , assuming that pores are spherical [27]:

$$\lambda = D \left( \frac{2V_s}{3(1-V_s)} \right) \quad (3)$$

The top graph in Figure 4 shows the plot of  $\rho_d$  against  $\lambda$  calculated from the (yield) stress 0.2% plastic strain using these equations, for samples from each of the three treatments. The plot agrees (within experimental error typical of investigations on metal foams) in each series with a linear relation. This is as expected if the size effect is attributable to Taylor hardening from an emission of geometrically necessary dislocations. The equations of the linear regression lines of best fit are given on the graph.

The slope for the samples taken through Treatment 1 (annealing) is slightly negative and, comparatively, of small value; within experimental error this is consistent with an absence of a size effect in these samples. With Treatments 2 and 3 (conventional infiltration processing and cooling during the composite stage), a clear size effect is seen, with the magnitude measurably increased by the cooling step in Treatment 3: the slope is higher by a factor of almost 4. All data thus confirm the above interpretation.

The density of dislocations induced by the thermal expansion mismatch can be estimated by finding an expression for the density of dislocations,  $\rho_T$  with Burgers vector  $b$  needed to compensate for a volumetric strain mismatch  $\Delta e_V$  (which, if caused by differing thermal expansion, is  $3 \Delta \text{CTE} \Delta T$ ) between hard spherical particles of diameter  $D$  and volume fraction  $1-V_s$ , assuming that dislocations are emitted as loops of diameter  $D/\sqrt{2}$ :

$$\rho_T = \frac{2\sqrt{2}\Delta e_V (1-V_s)}{bD V_s} \quad (4)$$

This equation can be used to predict the expected slope of the  $\rho_T$  against  $1/\lambda$  plots for Treatments 2 and 3, where in the first case the thermal excursion is taken as being 200 K (assuming as in Ref. [28] that above approximately 500K dislocations will be removed by annealing in pure aluminium) and for the second 600K (from approximately 500K down to 77K then back to room temperature, assuming that the effect of both positive and negative temperature changes is additive). This gives predicted slopes of  $1 \times 10^8 \text{ m}^{-1}$  for Treatment 2 and  $3 \times 10^8 \text{ m}^{-1}$  for Treatment 3, to be compared respectively with experimental values of  $3.4 \times 10^7$  and  $1.2 \times 10^8 \text{ m}^{-1}$  respectively, see Fig. 4. Measured slopes are thus roughly one-third the predicted values, while the relation between them (a factor of 3) is similar. That the values of dislocation density predicted by this simple approach should too large can be explained by several arguments: the model assumes hard spheres and perfect interfacial adhesion, whereas some of the mismatch will be taken up by elastic deformation,

and stresses could be relieved in part by interfacial NaCl/Al decohesion. Also, the model is very simple, given that it assumes simple circular dislocation loop emission and neglects the effect of work hardening during emission (known to affect the dislocation punching process [29]).

The exercise was repeated for the measured microcellular aluminium flow stress  $\sigma^*$  values at 2 or 5% strain, after correcting  $\sigma^*$  for the effect of internal damage using Eq. 4 of Ref. [30] (i.e., using Lemaître's approximation, which equates the fractional damage-induced decreases in flow stress or Young's modulus) [24]. One obtains the two lower plots in Fig. 4. As seen the result is qualitatively similar as for the flow stress: the annealed samples still show no size effect, while samples initially hardened by thermal dislocations (Treatments 2 or 3) again give a linear relation. The slope, however, is greater by roughly an order of magnitude compared with data for the yield stress (Fig. 4, top).

The strong increase in  $\rho_d$  that this implies is interesting, given how small the strains are (2 and 5%). Being absent in the annealed samples the effect is not caused by strain gradients (a simple bending-beam back-of-the-envelope calculation confirms this [24]). High work hardening rates in fine-scale replicated pure aluminium thus also have their origin in thermal dislocations present before samples yield. These dislocations either multiply at a very high rate, or alternatively pile-up against barriers, creating a back-stress in the matrix, which in turn will raise the apparent metal rate of work hardening (and back-calculated  $\rho_d$  values). The obvious barrier to dislocation motion is here the oxide layer covering the pore surface, known to influence strongly the strength of replicated microcellular aluminium, particularly if samples are produced (as here) by dissolution in simple water [17]. This interpretation is also consistent with the relatively straight post-yield stress-strain curves displayed with finer pores, Fig. 2, which suggest kinematic (or back-stress) hardening, and with observations made recently on surface-coated FIB-milled micropillars [3, 31, 32].

In conclusion, evidence is presented for a plasticity size effect in replicated microcellular high-purity aluminium. Three thermal treatments show that size-dependence in the microcellular metal yield stress is dislocational, and has its origin in thermal dislocation emission during the manufacturing process. A simple model of the density of dislocations thus injected into the metal explains the scale-dependent 0.2% offset yield stress of replicated microcellular aluminium. Rates of work hardening after further deformation of the material also increase as the pore size decreases. This work-hardening size effect would require a deeper investigation to be fully understood; what emerges here is that it is likely linked with image forces along the many free surfaces present within the material when its pores fall below roughly 100  $\mu\text{m}$  in diameter.

## Acknowledgments

This work was funded by the Swiss National Science Foundation, Project No. 200020-1182134.

## References

- [1] N.A. Fleck, G.M. Muller, M.F. Ashby, J.W. Hutchinson, *Acta Metallurgica et Materialia*, 42 (1994) 475-487.
- [2] M.D. Uchic, P.A. Shade, D.D. Dimiduk, *Annual Review of Materials Research*, 39 (2009) 361-386.
- [3] J.R. Greer, J.T.M. De Hosson, *Progress in Materials Science*, 56 (2011) 654-724.
- [4] W.D. Nix, H. Gao, *Journal of the Mechanics and Physics of Solids*, 46 (1998) 411-425.
- [5] E. Arzt, *Acta Materialia*, 46 (1998) 5611.
- [6] E. Arzt, G. Dehm, P. Gumbsch, O. Kraft, D. Weiss, *Progress in Materials Science*, 46 (2001) 283.
- [7] R.B. Calhoun, D.C. Dunand, Chapter 3.02 - Dislocations in Metal Matrix Composites, in: T.W. Clyne (Ed.) *Comprehensive Composite Materials*, Vol. 3: Metal Matrix Composites, Pergamon, Oxford UK, 2000, pp. 27-59.

- [8] M. Kouzeli, A. Mortensen, *Acta Materialia*, 50 (2002) 39-51.
- [9] D. Mordehai, S.-W. Lee, B. Backes, D.J. Srolovitz, W.D. Nix, E. Rabkin, *Acta Materialia*, 59 (2011) 5202-5215.
- [10] L.B. Freund, S. Suresh, *Thin Film Materials, Stress, Defect Formation and Surface Evolution*, Cambridge University Press, Cambridge, UK, 2003.
- [11] R. Goodall, A. Mortensen, *Porous Metals*, in: K. Hono, D. Laughlin (Eds.) *Physical Metallurgy: 5th Edition*, Elsevier, Amsterdam, NL, 2013, pp. (in print).
- [12] Y. Conde, J.F. Despois, R. Goodall, A. Marmottant, L. Salvo, C. SanMarchi, A. Mortensen, *Advanced Engineering Materials*, 8 (2006) 795-803.
- [13] J.F. Despois, Y. Conde, C.S. Marchi, A. Mortensen, *Advanced Engineering Materials*, 6 (2004) 444-447.
- [14] R. Goodall, J.F. Despois, A. Marmottant, L. Salvo, A. Mortensen, *Scripta Materialia*, 54 (2006) 2069.
- [15] R. Goodall, A. Marmottant, L. Salvo, A. Mortensen, *Materials Science and Engineering: A*, 465 (2007) 124-135.
- [16] F. Diologent, R. Goodall, A. Mortensen, *Acta Materialia*, 59 (2011) 6869-6879.
- [17] F. Diologent, R. Goodall, A. Mortensen, *Acta Materialia*, 57 (2009) 286-294.
- [18] L.J. Gibson, M.F. Ashby, *Cellular Solids - Structure and Properties - Second Ed.*, Cambridge University Press, Cambridge, U.K., 1997.
- [19] M.F. Ashby, A. Evans, N.A. Fleck, L.J. Gibson, J.W. Hutchinson, H.N.G. Wadley, *Metal Foams: A Design Guide*, Butterworth Heinemann, Boston USA, 2000.
- [20] C. San Marchi, A. Mortensen, *Acta Materialia*, 49 (2001) 3959-3969.
- [21] J.F. Despois, R. Mueller, A. Mortensen, *Acta Materialia*, 54 (2006) 4129-4142.
- [22] D.W. Kaufmann, Chapter 25 - Physical properties of sodium chloride in crystal, liquid, gas and aqueous solution states, in: D.W. Kaufmann (Ed.) *Sodium chloride, the production and properties of salt and brine*, Reinhold Publishing Corporation, New York, 1960, pp. 587-626.
- [23] D.R. Lide, in, CRC Press, Boca Raton, Fla., USA, 1992.
- [24] J.-F. Despois, in: *Institute of Materials, Ecole Polytechnique Fédérale de Lausanne*, 2005.
- [25] N. Hansen, *Acta Metallurgica*, 25 (1977) 863-869.
- [26] E.A. Brandes, G.B. Brook, *Smithells Metals Reference Book, Seventh Edition, 7th ed.*, Butterworth-Heinemann, Woburn MA, 1992.
- [27] A. Mortensen, M.C. Flemings, *Metallurgical Transactions*, 27A (1996) 595-609.
- [28] J.A. Isaacs, A. Mortensen, *Metallurgical Transactions*, 23A (1992) 1207-1219.
- [29] D.C. Dunand, A. Mortensen, *Acta Metallurgica et Materialia*, 39 (1991) 127-139.
- [30] C. San Marchi, J.F. Despois, A. Mortensen, *Acta Materialia*, 52 (2004) 2895-2902.
- [31] R. Gu, A.H.W. Ngan, *Acta Materialia*, 60 (2012) 6102-6111.
- [32] A.T. Jennings, C. Gross, F. Greer, Z.H. Aitken, S.W. Lee, C.R. Weinberger, J.R. Greer, *Acta Materialia*, 60 (2012) 3444-3455.

### List of figures

Figure 1 – Scanning Electron Microscope images of (a) foam with 25 $\mu$ m mean pore diameter and porosity of 80%, and (b) foam with 400 $\mu$ m mean pore diameter and porosity of 85%. Struts that intersect with the cut surface are indicated in red.

Figure 2 – Example compressive stress-strain curves obtained for replicated aluminium foams of different mean pore size but similar density.

Figure 3 – Schematic diagram depicting the 3 heat treatment routes used.

Figure 4 – Back-calculated global density of dislocations,  $\rho_d$ , in the aluminium of the different metal foams and treatments examined here at three values of plastic strain: 0.2% (top), 2% (middle), 5% (bottom), versus mean free path in the matrix,  $\lambda$ . Linear best fit lines and equations are indicated.

## FIGURES

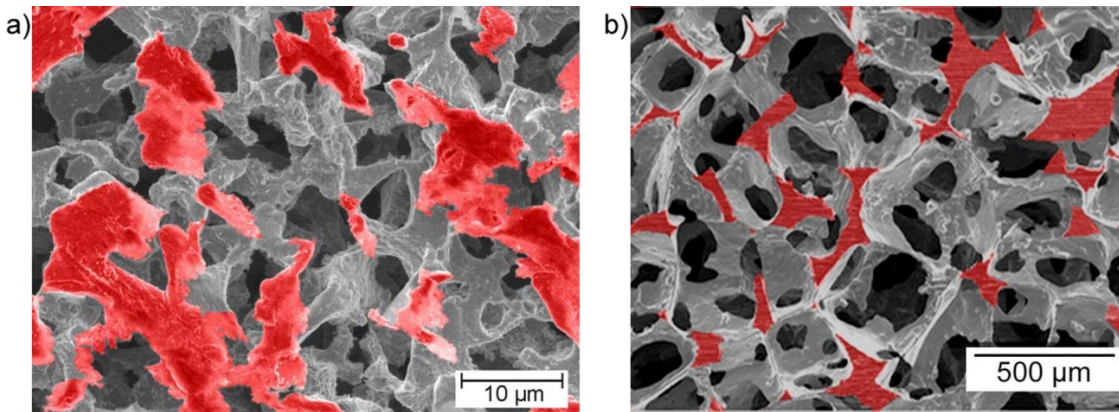


Figure 1 – Scanning Electron Microscope images of (a) foam with 25 $\mu$ m mean pore diameter and porosity of 80%, and (b) foam with 400 $\mu$ m mean pore diameter and porosity of 85%. Struts that intersect with the cut surface are indicated in red.

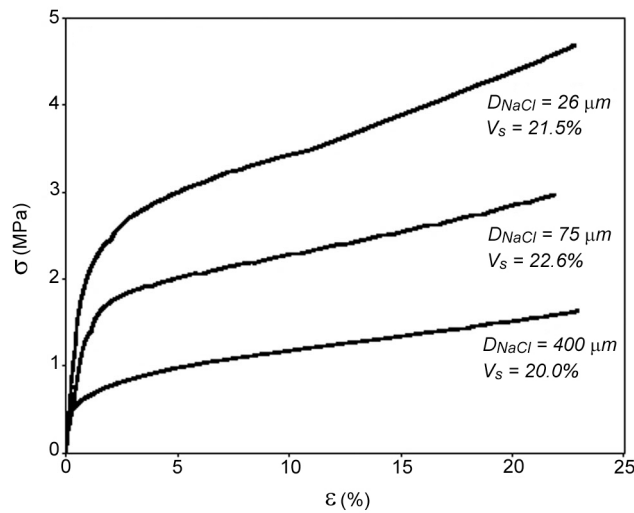


Figure 2 – Example compressive stress-strain curves obtained for replicated aluminium foams of different mean pore size but similar density.

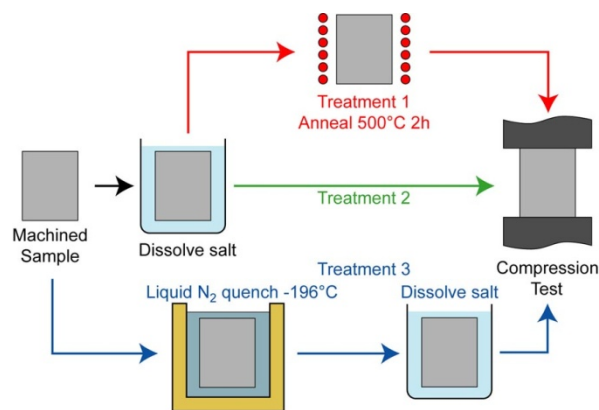


Figure 3 – Schematic diagram depicting the 3 heat treatment routes used.

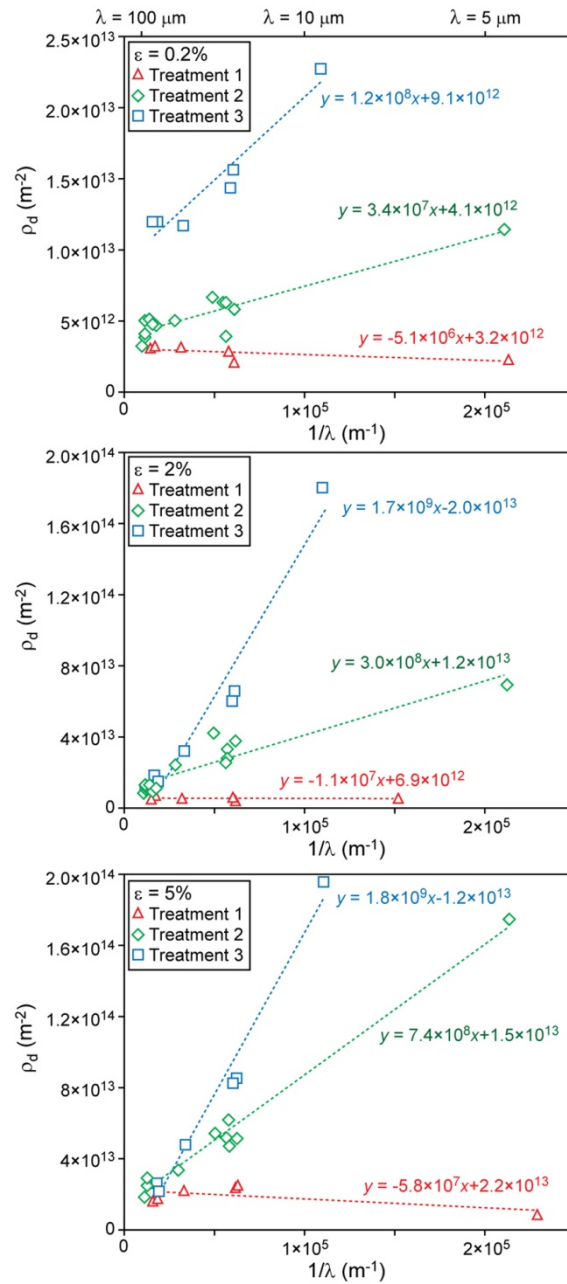


Figure 4 – Back-calculated global density of dislocations,  $\rho_d$ , in the aluminium of the different metal foams and treatments examined here at three values of plastic strain: 0.2% (top), 2% (middle), 5% (bottom), versus mean free path in the matrix,  $\lambda$ . Linear best fit lines and equations are indicated.